THE JOURNAL OF PHYSICAL CHEMISTRY C

Article

pubs.acs.org/JPCC

Photoluminescence Enhancement of Silicon Quantum Dot Monolayer by Double Resonance Plasmonic Substrate

Asuka Inoue, Hiroshi Sugimoto, and Minoru Fujii*

Department of Electrical and Electronic Engineering, Graduate School of Engineering, Kobe University, Rokkodai, Nada, Kobe 657-8501, Japan

Supporting Information

ABSTRACT: A structure composed of a monolayer of luminescent silicon quantum dots (Si-QDs) and a silver (Ag) film over nanosphere (AgFON) plasmonic nanostructure is prepared by precisely controlling the distance. A AgFON structure modifies both the photoluminescence (PL) and the PL excitation (PLE) spectra of a Si-QD monolayer significantly. It is shown that the spectral shape is very sensitive to the spacer thickness and the wavelength dependence of the PL and PLE enhancement factors agrees well with the absorptance spectra. Due to multiple surface plasmon resonances of a AgFON structure, in proper spacer thicknesses, simultaneous enhancements of the excitation cross section and the emission rate are achieved. In the wavelength range where the absorption cross section of Si-QDs is small, the PL enhancement factor averaged in a relatively wide region (10×10 mm^2) reaches 12.

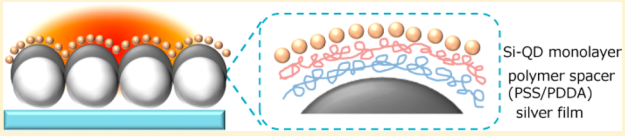

INTRODUCTION

Semiconductor quantum dots (QDs) have been attracting a great deal of attention as a nanolight emitter because of their excellent characteristics such as tunable luminescence wavelength, high photostability, and high chemical stability.[1−3] These potentially superior properties of QDs compared to other phosphors such as fluorescent protein and organic dyes[4] make them a promising material for applications in biophotonic[5−7] and optoelectronic devices.[8−10] However, toxic heavy metal elements in commercially available cadmium (Cd)- or lead (Pb)-chalcogenide QDs have been an obstacle for the widespread usage, especially in a biomedical field.[11]

Among various heavy-metal-free QDs developed so far,[12] silicon (Si) QDs have several advantages such as the high environmental friendliness and the high compatibility with the existing Si-based electronic device technologies. In the past decade, the fabrication process of Si-QDs has been developed very rapidly, and now very high quality Si-QDs are available.[13,14] The highest photoluminescence (PL) quantum yield (QY) reaches 70% at 775 nm.[15] By using these Si-QDs, thin film transistors,[16] light emitting diodes,[17] and solar cells[18] are produced. However, despite the recent rapid progress, there still remain several intrinsic problems to be solved to make Si-QDs a practically useful material. The largest problem is the small absorption cross section in the visible and near-infrared (NIR) spectral ranges due to the indirect nature of the energy band structure. For the efficient excitation, Si-QDs should be excited above the direct band gap (~3.4 eV);[19] the wavelength range is not compatible with many biomedical applications.

A promising approach to overcome the problem is utilizing the coupling with surface plasmon resonances of metal nanostructures. Different structures have been proposed to achieve efficient coupling between Si-QDs and a metal nanostructure. At the beginning, a metal nanostructure was placed near Si-QDs embedded in solid matrixes.[20−25] Recently, a composite nanoparticle composed of Si-QDs and a metal nanostructure such as a nanoparticle[26−28] and a nanorod[29] have been developed by using electrostatic attraction,[27,29] chemical bonding,[28] and DNA hybridization.[28] An attempt to place a monolayer of Si-QDs in a plasmonic nanogap is also reported.[30] In these previous structures, the PL enhancement is due to either the enhancement of the absorption cross section or that of the emission rate depending on the relation between the surface plasmon resonance wavelength and the PL wavelength.

The purpose of this work is to develop a structure to simultaneously enhance the absorption cross section and emission rate of Si-QDs to obtain high PL intensity, especially under excitation by long wavelength photons. Although the concept of double resonance has widely been employed in surface enhanced Raman scattering (SERS),[31] it has not been applied to metal enhanced fluorescence (MEF) of Si-QD-based systems. To achieve the double resonance in Si-QD-based systems, metal nanostructures should be designed to have multiple surface plasmon resonances in a wide wavelength range. In this work, we employ a silver (Ag) film over nanosphere (AgFON) structure, which has been widely used for SERS[32,33] and MEF,[34,35] as a plasmonic substrate with multiple resonances. In order to maximize the luminescence enhancement, the distance between a plasmonic substrate and a Si-QD monolayer should be controlled very precisely. We develop a process to place a monolayer of Si-QDs by controlling the distance by a polymer spacer grown by a

Received: January 23, 2017
Revised: May 8, 2017
Published: May 9, 2017

DOI: 10.1021/acs.jpcc.7b00717
J. Phys. Chem. C 2017, 121, 11609−11615

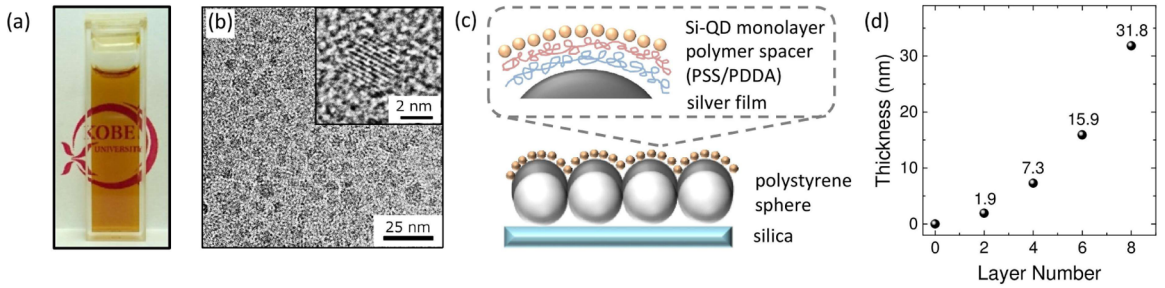

Figure 1. (a) Photograph of a colloidal solution (methanol solution) of B and P codoped Si-QDs. (b) TEM image of a Si-QD monolayer. Inset is a high resolution TEM image of a Si-QD. (c) Schematic illustration of a AgFON structure with a Si-QD monolayer on the surface. (d) Thickness of polymer layer measured by spectroscopic ellipsometry.

layer-by-layer (LbL) assembly process.[36−38] We show that a AgFON structure modifies both the PL and PL excitation (PLE) spectra of a Si-QD monolayer significantly, and that the wavelength dependence of the PL and PLE enhancement factors agrees well with the absorptance spectra. In the wavelength range where the absorption cross section of Si-QDs is small, the enhancement factor averaged in a wide region (10×10 mm^2) reaches 12.

RESULT AND DISCUSSION

As a precursor for the preparation of a Si-QD monolayer, we employ a colloidal solution of all-inorganic Si-QDs developed in our group.[39−41] The Si-QDs have a heavily boron (B) and phosphorus (P) doped thin layer on the surface, which induces negative potential on the surface (zeta potential: −40 mV at pH 7)[39] and makes the QDs dispersible in polar solvents without any surface functionalization processes.[40,42] Figure 1a shows a photograph of a colloidal solution of codoped Si-QDs. The solution is very clear, and light scattering by agglomerates is not observed. Figure 1b shows a transmission electron microscope (TEM) image of a Si-QD layer prepared by drop-casting the diluted methanol solution on a carbon-coated Cu mesh. A densely packed monolayer of Si-QDs is formed, and no three-dimensional agglomerates are observed. The lattice fringe in the high-resolution image corresponds to {111} planes of Si crystal.

Figure 1c shows a schematic illustration of the structure studied in this work. A two-dimensional array of polystyrene spheres (350 nm in diameter) is formed on a silica substrate, followed by vacuum evaporation of a Ag film (200 nm in thickness). The AgFON substrate is then immersed in 6-amino-1-hexanethiol, hydrochloride (6-AHT) ethanol solution (1 mM) for the formation of a self-assembled monolayer (SAM) with a positively charged amine group on the surface. The thickness of SAM is about 1.2 nm.[43] On the AgFON substrate, a polymer spacer is formed by the LbL assembly process; i.e., negatively and positively charged polymers are deposited alternatively (see Methods). In this work, the layer number is changed from 0 to 8. In Figure 1d, the thickness of the polymer layer measured by spectroscopic ellipsometry is plotted as a function of the layer number. Hereafter, we denote AgFON with n number of polymer layers as L(n)/AgFON. A monolayer of Si-QDs is formed on a positively charged surface, i.e., L(n)/AgFON with even n, by drop-casting a diluted colloidal solution of Si-QDs (0.17 mg/mL). Formation of a monolayer of Si-QDs is confirmed by spectroscopic ellipsometry (Figure S1).[44] We denote the structure with a Si-QD monolayer as Si-QD/L(n)/AgFON.

Figure 2a shows absorptance spectra of L(n)/AgFON (n = 0−6) and Si-QD/L(6)/AgFON. The absorptance is defined by

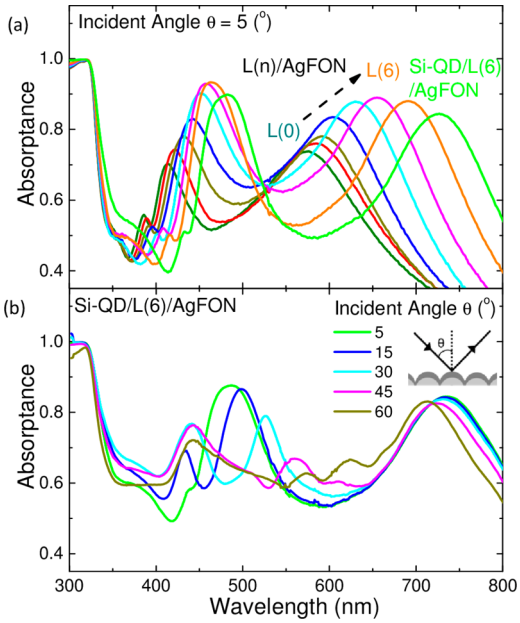

Figure 2. (a) Absorptance spectra of L(n)/AgFON (n = 0−6) and Si-QD/L(6)/AgFON. The incident angle (θ) is 5°. (b) Absorptance spectra of Si-QD/L(6)/AgFON measured at different incident angles (θ = 5−60°).

$1 - T - R$, where T and R are transmittance and reflectance, respectively. In this work, the transmittance is zero for all the samples in the whole wavelength range. Therefore, the absorptance spectra are obtained by simply subtracting reflectance spectra from one. In Figure 2a, two broad bands are seen around 400−500 nm and 600−800 nm. Both bands shift to longer wavelength with increasing the layer number n. The red shift is due to the increase of the dielectric constant around metal nanostructures supporting the surface plasmon. Further red shift is observed by placing a Si-QD monolayer on the top (Si-QD/L(6)/AgFON), also due to the increase of the dielectric constant. Note that the absorption by a Si-QD monolayer is negligibly small and does not affect the spectral shape.

Figure 2b shows absorptance spectra of Si-QD/L(6)/AgFON measured at different incident angles (θ = 5−60°). The long-wavelength band is insensitive to θ, indicating that this is due to localized surface plasmon resonances of Ag nanostructures in AgFON. On the other hand, the short-

DOI: 10.1021/acs.jpcc.7b00717
J. Phys. Chem. C 2017, 121, 11609−11615

wavelength band splits into two bands and the splitting increases with θ, suggesting that the band arises from surface plasmon polaritons with dispersion relations. Absorptance rising below 350 nm is due to the interband transition of Ag.

Figure 3a shows absorptance spectra of Si-QD/L(n)/AgFON with n changed from 0 to 8. Since a Si-QD monolayer can be

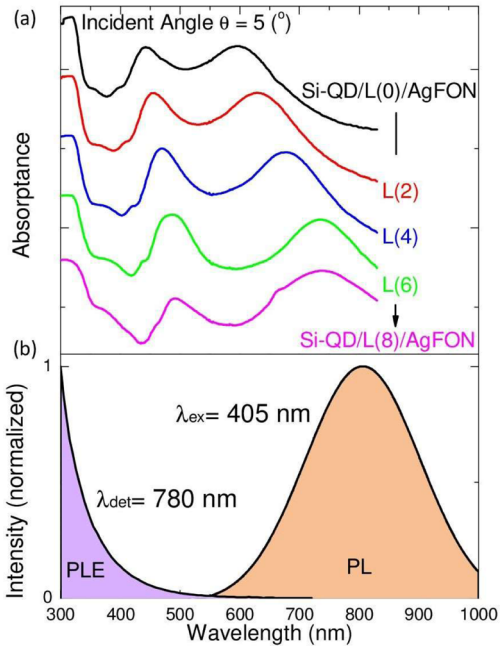

Figure 3. (a) Absorptance spectra of Si-QD/L(n)/AgFON with different number (n) of polymer layers. The incident angle (θ) is 5°. (b) A PL spectrum excited at 405 nm (orange) and a PLE spectrum detected at 780 nm (purple) of a Si-QD monolayer on a silica substrate.

formed only on positively charged polymer, n is even numbers. The spectral shape depends on n. The overall red shift of the peaks with increasing n can be explained by the increased dielectric constant around Ag nanostructures. Figure 3b shows a PL spectrum excited at 405 nm and a PLE spectrum detected at 780 nm of a Si-QD monolayer on a silica substrate. The PLE spectrum decreases rapidly with increasing the wavelength due to the indirect transition of Si crystal in the visible range. Therefore, to excite Si-QDs efficiently, UV light is necessary, which is one of the serious drawbacks of Si-QDs for the biophotonics applications. By comparing Figure 3a,b, we notice that there are surface plasmon resonance bands in the weak absorption region of Si-QDs and thus we may achieve the excitation cross-section enhancement. At the same time, the long wavelength bands due to localized surface plasmon resonances overlap with the emission band. Therefore, we can expect to enhance the emission rate, simultaneously.

Figure 4a shows PL spectra of Si-QD/L(n)/AgFON excited at 405 nm. The incident angle of the excitation light is 45°. The spectra of a Si-QD monolayer on a silica substrate and a flat Ag film are also shown as references. The PL intensity on a flat Ag film is about 30% quenched from that on a silica substrate due to the dissipation to the surface plasmon polaritons. Note that Si QDs are not directly attached to Ag because of SAM (~1.2 nm). This results in relatively small PL quenching on a flat Ag film. Compared to a Si-QD monolayer on a silica substrate and on a flat Ag film, the PL intensity of Si-QD/L(n)/AgFON is

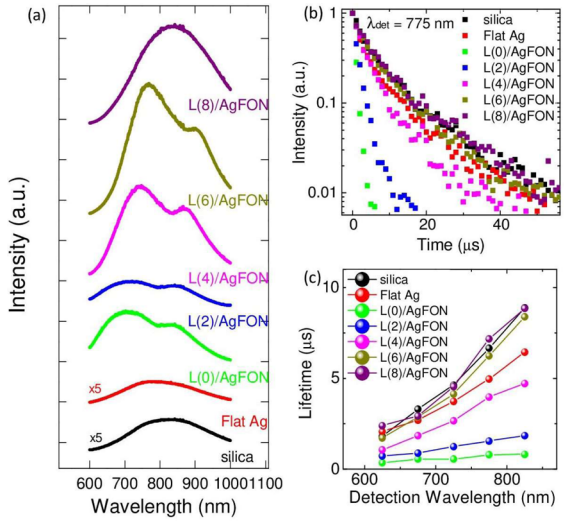

Figure 4. (a) PL spectra of a Si-QD monolayer on a silica substrate, a flat Ag film, and L(n)/AgFON. (b) PL decay curves detected at 775 nm. (c) PL lifetimes as a function of detection wavelength. The excitation wavelength is 405 nm. The incident angle (θ) is 45°.

strongly enhanced and the spectral shape is largely modified. Especially in Si-QD/L(4)/AgFON and Si-QD/L(6)/AgFON, new narrow bands appear around 750 nm. The drastic modification of the spectral shape indicates that the emission process of Si-QDs is strongly modified by the AgFON structures. We will discuss the PL spectral shape of Si-QD/L(n)/AgFON more in detail by comparing it with a corresponding absorptance spectrum later.

Figure 4b shows PL decay curves of Si-QD/L(n)/AgFON detected at 775 nm. The excitation and detection geometry is the same as that of the PL spectra measurements. The excitation source is a modulated 405 nm laser. We can see that the PL lifetime is significantly shortened by the AgFON structure. In Figure 4c, the PL lifetime obtained by fitting the decay curves by the stretched exponential function $I = I_0 \exp\{(-(t/\tau)^{\beta}\}$, where τ is the decay constant and β is the stretching parameter, is plotted as a function of a detection wavelength. The average PL lifetime (τ_{ave}) is defined as $\tau_{ave} = \tau\beta^{-1}\Gamma_E(\beta^{-1})$, where Γ_E is the Euler gamma function.[45] The lifetime is the longest on a silica substrate and is shortened on a flat Ag film due to the coupling with the surface plasmon polaritons. The lifetime is the shortest in Si-QD/L(0)/AgFON, suggesting the most efficient coupling between the emission of Si-QDs and the surface plasmons of the AgFON structure. With increasing the polymer thickness, i.e., with increasing n in Si-QD/L(n)/AgFON, the lifetime becomes long, and in Si-QD/L(8)/AgFON, it is almost the same as that of Si-QDs on a silica substrate. This is consistent with the fact that the PL spectral shape is not strongly modified in Si-QD/L(8)/AgFON in Figure 4a. In this case, the PL enhancement is mainly due to the enhancement of the absorption cross section.

In the AgFON structures studied in this work, due to the existence of multiple surface plasmon resonances, both the excitation and the emission processes are considered to be affected. In that case, an emission−excitation contour is a convenient figure to overlook the whole enhancement process. Figure 5a,b shows the emission−excitation contours of a Si-QD monolayer on a silica substrate and Si-QD/L(6)/AgFON. The data of Si-QD/L(n)/AgFON with other n are shown in the Supporting Information (Figure S2). The incident angle of

DOI: 10.1021/acs.jpcc.7b00717
J. Phys. Chem. C 2017, 121, 11609−11615

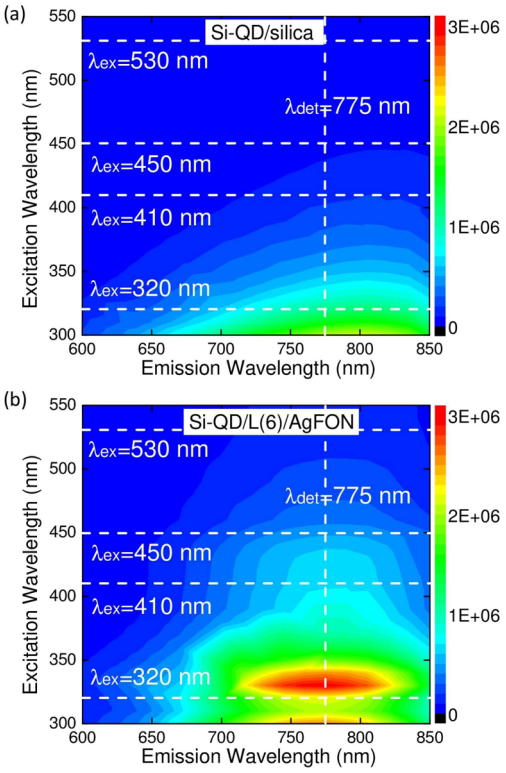

Figure 5. Emission−excitation contours of (a) a Si-QD monolayer on a silica substrate and (b) Si-QD/L(6)/AgFON. The incident angle (θ) is 60°.

excitation light is 60°. The color scales are the same in the two figures. On a silica substrate, Si-QDs are most efficiently excited at the shortest wavelength, which is consistent with Figure 3b. A similar trend can be seen in Si-QD/L(6)/AgFON from the longest excitation wavelength to 330 nm. In the excitation wavelength range, the PL intensity is strongly enhanced and thus the wavelength range for efficient excitation of Si QDs is largely extended to longer wavelength. Below 320 nm, no further increase of the intensity is observed. This is due to the onset of the interband transitions of Ag and the loss of the metallic character. The very strong modification of the contours is direct evidence that both the absorption and the emission processes of Si-QD are modified by the AgFON structures.

To scrutinize the enhancement processes more in detail, we obtain PL enhancement factor spectra by dividing the PL spectra of Si-QD/L(n)/AgFON (n = 0, 2, 4, 6, 8) by those of a Si-QD monolayer on a silica substrate. In Figure 6, the PL enhancement factor spectra for Si-QD/L(n)/AgFON (n = 0, 2, 4, 6, 8) obtained for 4 different excitation wavelengths (320, 410, 450, and 530 nm) are shown by colored solid curves. The PL spectra are extracted from the emission−excitation contours, and the excitation wavelengths correspond to horizontal broken lines in Figure 5. In Figure 6, the absorptance spectra are also shown to discuss the correlation between the PL enhancement factor and absorptance spectra. In Figure 6a (Si-QD/L(0)/AgFON), when the excitation wavelength is 320 nm, the luminescence is severely quenched, i.e., enhancement factor ≪ 1. The situation is slightly calmed in Si-QD/L(2)/AgFON (Figure 6b), in which the distance between a Si-QD monolayer and a AgFON structure is ∼1.9 nm. The PL enhancement factor under 320 nm excitation slowly increases with n and reaches a maximum (∼2) at n = 6 (Figure 6d), in which the distance is ∼15.9 nm. Since the enhancement of excitation cross section is not expected at 320 nm due to the

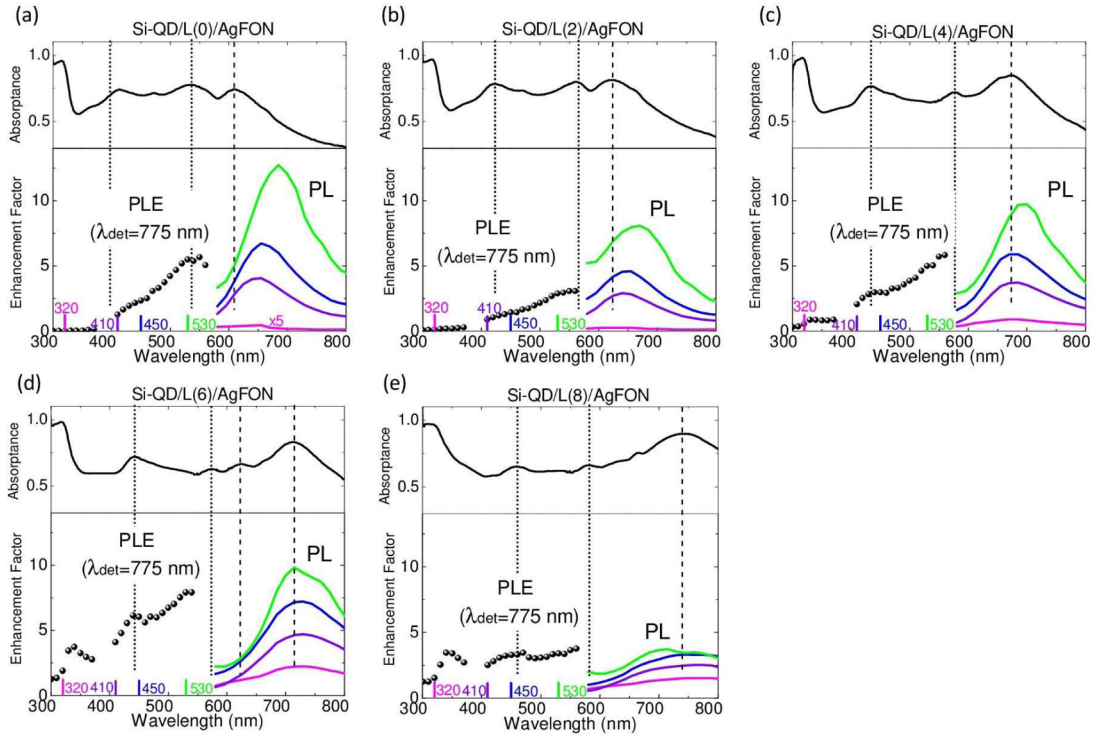

Figure 6. Absorptance spectra (black solid curves) and enhancement factor spectra of PL excited at 320, 410, 450, and 530 nm (colored solid curves) and those of PLE detected at 775 nm (filled circles) of Si-QD/L(n)/AgFON. Panels (a−e) correspond to n = 0, 2, 4, 6, and 8. The incident angle (θ) is 60°.

DOI: 10.1021/acs.jpcc.7b00717
J. Phys. Chem. C 2017, 121, 11609−11615

onset of the interband transition of Ag, the observed small enhancement at $n = 6$ arises mainly from the emission rate enhancement and resultant quantum yield enhancement.

On the other hand, when the excitation wavelength is longer than ~400 nm, we can see the luminescence enhancement not only in large n, but also in Si-QD/L(0)/AgFON. In all n, the enhancement factor increases with increasing the excitation wavelength. The wavelength of the maximum PL enhancement depends on n and shifts to longer wavelength with increasing n, being consistent with the long wavelength shift of the longest wavelength absorptance peak with n. In particular, in $n = 4$ and 6, the peak wavelengths of the PL enhancement factor spectra and the absorptance spectrum agree very well. This is an evidence that the radiative decay rates of Si-QDs are strongly enhanced by the AgFON structure. The enhancement factor is the largest (~12) in Si-QD/L(0)/AgFON under 530 nm excitation (Figure 6a, green solid curve). It is noted that the PL is obtained from a relatively wide region (10×10 mm^2) and thus the observed enhancement factor is the averaged one in the region.

The observed strong excitation wavelength dependence of the enhancement factor in Figure 6 indicates that the enhancement of the excitation cross section also plays a major role for the luminescence enhancement. This can be seen more clearly in the PLE enhancement factor spectra obtained by dividing the PLE spectra of Si-QD/L(n)/AgFON (n = 0, 2, 4, 6, 8) detected at 775 nm with that of a Si-QD monolayer on a silica substrate (filled circles in Figure 6). In all the samples, the features in the PLE enhancement factor spectra agree very well with the peaks in the absorptance spectra as shown by vertical broken lines. For example, in Si-QD/L(6)/AgFON (Figure 6d), a peak can clearly be seen around 440 nm in both spectra. As described above, the excitation cross-section enhancement is larger at longer wavelength, where the intrinsic absorption cross section of Si-QDs is small. The large enhancement factor at long wavelength range is very beneficial for applications where long wavelength excitation is crucial.

CONCLUSION

We have succeeded in producing a AgFON structure with a monolayer of Si-QDs on the surface by controlling the distance very precisely. We found that both the PL spectra and the PLE spectra of Si-QDs are strongly modified by the structure and that excitation and emission properties are very sensitive to the distance between a Si-QD monolayer and AgFON. In optimum distances, the PL is enhanced ~12-fold in the excitation wavelength range where the intrinsic absorption cross section of Si-QDs is very small. Efficient excitation of Si-QDs in a long wavelength range is very important for the biophotonic and photovoltaic applications. The present results indicate that, despite the simple fabrication processes, a AgFON structure can be a versatile platform for the luminescence enhancement of Si-QDs if the distance is precisely controlled.

METHODS

Preparation of Colloidal Solution of Si-QDs. Colloidal Si-QDs were prepared by the method described in our previous papers.[40,42] Si-rich borophosphosilicate glass (BPSG) was deposited by cosputtering Si, SiO_2, B_2O_3, and P_2O_5 in an rf-sputtering apparatus. The films were peeled off from a substrate and annealed at 1100 °C in a N_2 gas atmosphere for 30 min to grow B and P codoped Si-QDs in BPSG matrixes. Si-QDs were isolated from BPSG matrixes by HF (46 wt %) etching and then redispersed in methanol.

Formation of AgFON Structure. A AgFON structure was prepared by using a 2D array of polystyrene nanospheres 350 nm in diameter (Polyscience, Polybead Polystyrene Microspheres). A 200 nm thick Ag film was deposited on the array of polystyrene nanospheres on a silica substrate by vacuum evaporation. A self-assembled monolayer (SAM) was formed onto the Ag film by immersing the substrate in a 1 mM ethanol solution of 6-amino-1-hexanethiol, hydrochroride (6-AHT) (Dojindo Molecular Technologies) for 24 h. This treatment results in the functionalization of the surface with a positively charged amine group. A polymer spacer was then formed by an LbL process.[37] A negatively charged polymer solution is an aqueous solution of 1 mg/mL poly(sodium 4-styrenesulfonate) (PSS) (Sigma-Aldrich, M_w = 70 000) containing 0.5 M NaCl, and a positively charged polymer solution is an aqueous 5 μL/ml poly(diallyldimethylammonium chloride) (PDDA) (Sigma-Aldrich, 20 wt % in water, M_w = 100 000−200 000) solution containing 0.5 M NaCl. The substrates were first immersed into the PSS solution for 20 min to adsorb a negatively charged polymer layer, and then immersed into the PDDA solution for 20 min to form a positively charged layer. This process was repeated to form multilayers. The final polymer layer must be a PDDA layer to make the surface positively charged.

Structural and Optical Characterization. TEM and high resolution TEM images were obtained by using JEM-2100F (JEOL) operating at 200 kV. The thickness of a polymer layer was measured by spectroscopic ellipsometry (HORIBA, Auto-SE). Refractive indices of 1.41 and 1.50 were used for the PDDA and PSS layers, respectively.[46] The optical transmittance and reflectance spectra were measured by a UV−vis−NIR spectrophotometer (Shimadzu, Solidspec 3700). The incident angle was changed from 5° to 60°. PL spectra and decay curves were obtained by using a single spectrometer equipped with a charge coupled device (CCD) and image-intensified CCD (Roper Scientific). The excitation source for the decay measurements is modulated 405 nm light (Coherent Inc., CUBE). The incident angle of excitation light is 45°. Emission−excitation contours were measured by a spectrofluorometer (Horiba Jovin Yvon, Fluorolog-3) equipped with a Xe lamp (450 W) and a double-grating monochromator as an excitation source. The incident angle of excitation light is 60°. The size of the excitation beam on a sample is about 10×10 mm^2.

ASSOCIATED CONTENT

Supporting Information

The Supporting Information is available free of charge on the ACS Publications website at DOI: 10.1021/acs.jpcc.7b00717.

Estimation of the thickness of Si-QD monolayer by spectroscopic ellipsometry; emission−excitation contours of Si-QD on silica, flat Ag, and L(n)/AgFON (PDF)

AUTHOR INFORMATION

Corresponding Author

*E-mail: fujii@eedept.kobe-u.ac.jp.

ORCID

Hiroshi Sugimoto: 0000-0002-1520-0940

Minoru Fujii: 0000-0003-4869-7399

DOI: 10.1021/acs.jpcc.7b00717
J. Phys. Chem. C 2017, 121, 11609−11615

Notes

The authors declare no competing financial interest.

■ ACKNOWLEDGMENTS

This work was partly supported by the 2015 JST Visegrad Group (V4)-Japan Joint Research Project on Advanced Materials and JSPS KAKENHI Grant Number 16H03828. H.S. acknowledges support from a Grant-in-Aid for JSPS Research Fellow (26-3120).

■ REFERENCES

(1) Hines, M. A.; Scholes, G. D. Colloidal PbS Nanocrystals with Size-Tunable Near-Infrared Emission: Observation of Post-Synthesis Self-Narrowing of the Particle Size Distribution. *Adv. Mater.* **2003**, *15*, 1844−1849.

(2) He, Y.; Lu, H. T.; Sai, L. M.; Su, Y. Y.; Hu, M.; Fan, C. H.; Huang, W.; Wang, L. H. Microwave Synthesis of Water-Dispersed CdTe/CdS/ZnS Core-Shell-Shell Quantum Dots with Excellent Photostability and Biocompatibility. *Adv. Mater.* **2008**, *20*, 3416−3421.

(3) He, Y.; Zhong, Y.; Peng, F.; Wei, X.; Su, Y.; Lu, Y.; Su, S.; Gu, W.; Liao, L.; Lee, S. T. One-Pot Microwave Synthesis of Water-Dispersible, Ultraphoto- and pH-Stable, and Highly Fluorescent Silicon Quantum Dots. *J. Am. Chem. Soc.* **2011**, *133*, 14192−14195.

(4) Resch-Genger, U.; Grabolle, M.; Cavaliere-Jaricot, S.; Nitschke, R.; Nann, T. Quantum Dots versus Organic Dyes as Fluorescent Labels. *Nat. Methods* **2008**, *5*, 763−775.

(5) Chan, W. C. W.; Nie, S. Quantum Dot Bioconjugates for Ultrasensitive Nonisotopic Detection. *Science* **1998**, *281*, 2016−2018.

(6) Michalet, X. Quantum Dots for Live Cells, in Vivo Imaging, and Diagnostics. *Science* **2005**, *307*, 538−544.

(7) Medintz, I. L.; Uyeda, H. T.; Goldman, E. R.; Mattoussi, H. Quantum Dot Bioconjugates for Imaging, Labelling and Sensing. *Nat. Mater.* **2005**, *4*, 435−446.

(8) Dolzhnikov, D. S.; Zhang, H.; Jang, J.; Son, J. S.; Panthani, M. G.; Shibata, T.; Chattopadhyay, S.; Talapin, D. V. Composition-Matched Molecular "solders" for Semiconductors. *Science* **2015**, *347*, 425−428.

(9) Kwak, J.; Bae, W. K.; Lee, D.; Park, I.; Lim, J.; Park, M.; Cho, H.; Woo, H.; Yoon, D. Y.; Char, K.; et al. Bright and Efficient Full-Color Colloidal Quantum Dot Light-Emitting Diodes Using an Inverted Device Structure. *Nano Lett.* **2012**, *12*, 2362−2366.

(10) Bozyigit, D.; Yarema, O.; Wood, V. Origins of Low Quantum Efficiencies in Quantum Dot LEDs. *Adv. Funct. Mater.* **2013**, *23*, 3024−3029.

(11) Tsoi, K. M.; Dai, Q.; Alman, B. A.; Chan, W. C. W. Are Quantum Dots Toxic? Exploring the Discrepancy Between Cell Culture and Animal Studies. *Acc. Chem. Res.* **2013**, *46*, 662−671.

(12) Xu, G.; Zeng, S.; Zhang, B.; Swihart, M. T.; Yong, K. T.; Prasad, P. N. New Generation Cadmium-Free Quantum Dots for Biophotonics and Nanomedicine. *Chem. Rev.* **2016**, *116*, 12234−12327.

(13) Dasog, M.; De Los Reyes, G. B.; Titova, L. V.; Hegmann, F. A.; Veinot, J. G. C. Size vs Surface: Tuning the Photoluminescence of Freestanding Silicon Nanocrystals Across the Visible Spectrum via Surface Groups. *ACS Nano* **2014**, *8*, 9636−9648.

(14) Mastronardi, M. L.; Maier-Flaig, F.; Faulkner, D.; Henderson, E. J.; Kübel, C.; Lemmer, U.; Ozin, G. A. Size-Dependent Absolute Quantum Yields for Size-Separated Colloidally-Stable Silicon Nanocrystals. *Nano Lett.* **2012**, *12*, 337−342.

(15) Sangghaleh, F.; Sychugov, I.; Yang, Z.; Veinot, J. G. C.; Linnros, J. Near-Unity Internal Quantum Efficiency of Luminescent Silicon Nanocrystals with Ligand Passivation. *ACS Nano* **2015**, *9*, 7097−7104.

(16) Holman, Z. C.; Liu, C. Y.; Kortshagen, U. R. Germanium and Silicon Nanocrystal Thin-Film Field-Effect Transistors from Solution. *Nano Lett.* **2010**, *10*, 2661−2666.

(17) Puzzo, D. P.; Henderson, E. J.; Helander, M. G.; Wang, Z.; Ozin, G. a.; Lu, Z. Visible Colloidal Nanocrystal Silicon Light-Emitting Diode. *Nano Lett.* **2011**, *11*, 1585−1590.

(18) Pi, X.; Zhang, L.; Yang, D. Enhancing the Efficiency of Multicrystalline Silicon Solar Cells by the Inkjet Printing of Silicon-Quantum-Dot Ink. *J. Phys. Chem. C* **2012**, *116*, 21240−21243.

(19) Wilson, W. L.; Szajowski, P. F.; Brus, L. E. Quantum Confinement in Size-Selected, Silicon Nanocrystals. *Science* **1993**, *262*, 1242−1244.

(20) Biteen, J. S.; Pacifici, D.; Lewis, N. S.; Atwater, H. a. Enhanced Radiative Emission Rate and Quantum Efficiency in Coupled Silicon Nanocrystal-Nanostructured Gold Emitters. *Nano Lett.* **2005**, *5*, 1768−1773.

(21) Biteen, J. S.; Sweatlock, L. a; Mertens, H.; Lewis, N. S.; Polman, A.; Atwater, H. a. Plasmon-Enhanced Photoluminescence of Silicon Quantum Dots: Simulation and Experiment Plasmon-Enhanced Photoluminescence of Silicon Quantum Dots: Simulation and Experiment. *J. Phys. Chem. C* **2007**, *111*, 13372−13377.

(22) Biteen, J. S.; Lewis, N. S.; Atwater, H. A.; Mertens, H.; Polman, A. Spectral Tuning of Plasmon-Enhanced Silicon Quantum Dot Luminescence. *Appl. Phys. Lett.* **2006**, *88*, 131109.

(23) Mochizuki, Y.; Fujii, M.; Hayashi, S.; Tsuruoka, T.; Akamatsu, K. Enhancement of Photoluminescence from Silicon Nanocrystals by Metal Nanostructures Made by Nanosphere Lithography. *J. Appl. Phys.* **2009**, *106*, 013517.

(24) Takeda, E.; Fujii, M.; Nakamura, T.; Mochizuki, Y.; Hayashi, S. Enhancement of Photoluminescence from Excitons in Silicon Nanocrystals via Coupling to Surface Plasmon Polaritons. *J. Appl. Phys.* **2007**, *102*, 023506.

(25) Imakita, K.; Fujii, M.; Nakamura, T.; Miura, S.; Takeda, E.; Hayashi, S. Enhancement of Radiative Recombination Rate of Excitons in Si Nanocrystals on Au Film. *Japanese J. Appl. Physics, Part 1 Regul. Pap. Short Notes Rev. Pap.* **2006**, *45*, 6132−6136.

(26) Harun, N. A.; Benning, M. J.; Horrocks, B. R.; Fulton, D. a. Gold Nanoparticle-Enhanced Luminescence of Silicon Quantum Dots Co-Encapsulated in Polymer Nanoparticles. *Nanoscale* **2013**, *5*, 3817−3827.

(27) Inoue, A.; Fujii, M.; Sugimoto, H.; Imakita, K. Surface Plasmon-Enhanced Luminescence of Silicon Quantum Dots in Gold Nanoparticle Composites. *J. Phys. Chem. C* **2015**, *119*, 25108−25113.

(28) Inoue, A.; Sugimoto, H.; Yaku, H.; Fujii, M. DNA Assembly of Silicon Quantum Dots/gold Nanoparticle Nanocomposites. *RSC Adv.* **2016**, *6*, 63933−63939.

(29) Sugimoto, H.; Chen, T.; Wang, R.; Fujii, M.; Reinhard, B. M.; Dal Negro, L. Plasmon-Enhanced Emission Rate of Silicon Nanocrystals in Gold Nanorod Composites. *ACS Photonics* **2015**, *2*, 1298−1305.

(30) Yashima, S.; Sugimoto, H.; Takashina, H.; Fujii, M. Fluorescence Enhancement and Spectral Shaping of Silicon Quantum Dot Monolayer by Plasmonic Gap Resonances. *J. Phys. Chem. C* **2016**, *120*, 28795−28801.

(31) Chu, Y.; Banaee, M. G.; Crozier, K. B. Double-Resonance Plasmon Substrates for Surface-Enhanced Raman Scattering with Enhancement at Excitation and Stokes Frequencies. *ACS Nano* **2010**, *4*, 2804−2810.

(32) Lin, W. C.; Liao, L. S.; Chen, Y. H.; Chang, H. C.; Tsai, D. P.; Chiang, H. P. Size Dependence of Nanoparticle-SERS Enhancement from Silver Film over Nanosphere (AgFON) Substrate. *Plasmonics* **2011**, *6*, 201−206.

(33) Zhang, X.; Van Duyne, R. P. Optimized Silver Film over Nanosphere Surfaces for the Biowarfare Agent Detection Based on Surface-Enhanced Raman Spectroscopy. *Mater. Res. Soc. Symp. Proc.* **2005**, *876*, R8.54.1−R8.54.6.

(34) Farcău, C.; Aştilean, S. Silver Half-Shell Arrays with Controlled Plasmonic Response for Fluorescence Enhancement Optimization. *Appl. Phys. Lett.* **2009**, *95*, 193110.

(35) Sugawa, K.; Tamura, T.; Tahara, H.; Yamaguchi, D.; Akiyama, T.; Otsuki, J.; Kusaka, Y.; Fukuda, N.; Ushijima, H. Metal-Enhanced Fluorescence Platforms Based on Plasmonic Ordered Copper Arrays: Wavelength Dependence of Quenching and Enhancement Effects. *ACS Nano* **2013**, *7*, 9997−10010.

DOI: 10.1021/acs.jpcc.7b00717
J. Phys. Chem. C 2017, 121, 11609−11615

(36) Kulakovich, O.; Strekal, N.; Yaroshevich, A.; Maskevich, S.; Gaponenko, S.; Nabiev, I.; Woggon, U.; Artemyev, M. Enhanced Luminescence of CdSe Quantum Dots on Gold Colloids. *Nano Lett.* **2002**, *2*, 1449−1452.
(37) Chan, Y.-H.; Chen, J.; Wark, S. E.; Skiles, S. L.; Son, D. H.; Batteas, J. D. Using Patterned Arrays of Metal Nanoparticles to Probe Plasmon Enhanced Luminescence of CdSe Quantum Dots. *ACS Nano* **2009**, *3*, 1735−1744.
(38) Cui, Q.; He, F.; Li, L.; Mohwald, H. Controllable Metal-Enhanced Fluorescence in Organized Films and Colloidal System. *Adv. Colloid Interface Sci.* **2014**, *207*, 164−177.
(39) Sugimoto, H.; Fujii, M.; Fukuda, Y.; Imakita, K.; Akamatsu, K. All-Inorganic Water-Dispersible Silicon Quantum Dots: Highly Efficient near-Infrared Luminescence in a Wide pH Range. *Nanoscale* **2014**, *6*, 122−126.
(40) Sugimoto, H.; Fujii, M.; Imakita, K.; Hayashi, S.; Akamatsu, K. All-Inorganic near-Infrared Luminescent Colloidal Silicon Nanocrystals: High Dispersibility in Polar Liquid by Phosphorus and Boron Codoping. *J. Phys. Chem. C* **2012**, *116*, 17969−17974.
(41) Sugimoto, H.; Fujii, M.; Imakita, K.; Hayashi, S.; Akamatsu, K. Codoping N- and P-Type Impurities in Colloidal Silicon Nanocrystals: Controlling Luminescence Energy from below Bulk Band Gap to Visible Range. *J. Phys. Chem. C* **2013**, *117*, 11850−11857.
(42) Sugimoto, H.; Fujii, M.; Fukuda, Y.; Imakita, K.; Akamatsu, K. All-Inorganic Water-Dispersible Silicon Quantum Dots: Highly Efficient near-Infrared Luminescence in a Wide pH Range. *Nanoscale* **2014**, *6*, 122−126.
(43) Klein, D. L.; Roth, R.; Lim, A. K. L.; Alivisatos, A. P.; McEuen, P. L. A Single-Electron Transistor Made from a Cadmium Selenide Nanocrystal. *Nature* **1997**, *389*, 699−701.
(44) Sugimoto, H.; Furuta, K.; Fujii, M. Controlling Energy Transfer in Silicon Quantum Dot Assemblies Made from All-Inorganic Colloidal Silicon Quantum Dots. *J. Phys. Chem. C* **2016**, *120*, 24469.
(45) Lindsey, C. P.; Patterson, G. D. Detailed Comparison of the Williams−Watts and Cole−Davidson Functions. *J. Chem. Phys.* **1980**, *73*, 3348.
(46) Ma, C.; Srinivasan, M. P.; Waring, A. J.; Lehrer, R. I.; Longo, M. L.; Stroeve, P. Supported Lipid Bilayers Lifted from the Substrate by Layer-by-Layer Polyion Cushions on Self-Assembled Monolayers. *Colloids Surf., B* **2003**, *28*, 319−329.

DOI: 10.1021/acs.jpcc.7b00717
J. Phys. Chem. C 2017, 121, 11609−11615